Trans. Phenom. Nano Micro Scales, 7(1): 53-61, Winter and Spring 2019
DOI: 10.22111/tpnms.2018.23378.1139

ORIGINAL RESEARCH PAPER

Dimensional analysis in the Study of Micro-Bubble Production Inside Venturi Tube

Mahin Ghannadi[1,], S. Fazlolah Saghravani[2], Hamid Niazmand[3]*

[1]*Ph.D. Student of Hydraulic Structures Shahrood University of Technology, Iran*
[2]*Associate Professor, Department of Civil Engineering, Shahrood University of Technology, Iran*
[3]*Professor of Mechanical Department, Ferdowsi University of Mashhad, Iran*

Received 5 January 2018; revised 1 December 2018; accepted 3 December 2018; available online 30 January 2019

ABSTRACT: The water and air flow and micro-bubble production inside the venturi tube is studied by dimensional analysis. Up to now, micro-bubble creation has been studied experimentally and no numerical analysis has been presented. Numerical analysis of micro-bubble creation in venturi tube requires fast computers and large amounts of storage space. To save time and storage space, dimensional analysis has been used. In this research, OpenFOAM and SPSS were used for numerical and statistical analysis, respectively. This study shows that the scalable model can be quite reliable for studying the pressure and velocity in the venturi tube. However, scaled models cannot be used to study alpha. Since the purpose of this research is to study micro-bubble formation in a Venturi tube and alpha, the scalable models cannot be used. Therefore, we need to simulate actual models in OpenFOAM software and study the formation of micro-bubbles, which is time-consuming and costly.

KEYWORDS*: Dimensional analysis; Micro-Bubble; OpenFOAM; Venturi tube*

INTRODUCTION

When the fluid flows through the throat section, the shrunken cross-section will accelerate the fluid accompanied by a pressure drop. This phenomenon is called as a Venturi effect, which will cause the fluid to occur a vacuum draw. In recent years, Venturi pipes have been widely applied in flow measurement, natural gas transmission, internal combustion engine pressurization system and industrial waste gas cleaning and dust removal. For example, in natural gas transmission, the use of Venturi tube jet-flow pressurization device achieves the mixture between a low pressure manufactured gas and a high pressure natural gas [1-2]. In industrial waste gas cleaning, the venturi scrubber is aimed at atomizing water by a high speed gas at the throat section to remove dust[3]. In internal combustion engine pressurization system, an exhaust gas recirculation technology in a pressurized diesel engine makes the exhaust gas circulation and flow driven by the vacuum degree at the throat section[4]. Quiroz-P´erez et al. studied theoretically that the of the gas production caused by the venturi tube in the gas well [5]. In a word, the application of venturi tube is helpful to effectively mix and improve chemical reaction, and thereby enhancing the energy efficiency. Therefore, to comprehend the fluid flow and pressure variation in the Venturi tube is of great significance for the realization of industrial energy saving.

✉ *Corresponding Author Email: *Mahin.gh@shahroodut.ac.ir*
Tel.: +989141303059; Note. This manuscript was submitted on January 5, 2018; approved on December 3, 2018; published online January 30, 2019.

Most practical fluid flow problems are too complex, both geometrically and physically, to be solved analytically. They must be tested by experimentally or approximated by computational fluid dynamics (CFD) [6]. These results are typically reported as experimental or numerical data points and smoothed curves. Such data have much more generality if they are expressed in compact, economic form. This is the motivation for dimensional analysis. The technique is a mainstay of fluid mechanics and is also widely used in all engineering fields plus the physical, biological, medical, and social sciences.

These results are typically reported as experimental or numerical data points and smoothed curves. Such data have much more generality if they are expressed in compact, economic form. This is the motivation for dimensional analysis.

The technique is a mainstay of fluid mechanics and is also widely used in all engineering fields plus the physical, biological, medical, and social sciences. [7].

Flow conditions for a model test are completely similar if all relevant dimensionless parameters have the same corresponding values for the model and the prototype. Instead of complete similarity, the engineering literature speaks of particular types of similarity, the most common being geometric, kinematic, dynamic, and thermal. Geometric similarity concerns the length dimension {L} and must be ensured before any sensible model testing can proceed.

	Nomenclature		
P	Static Pressure	ε	Energy dissipation
t	Time	ρ	Density
u	Average velocity	k	Turbulent kinetic energy
x, y, z	Coordinates	σ	Turbulent Prandtl numbers
Re	Reynolds number	μ_t	Turbulent viscosity
Eu	Euler number		**Subscripts**
	Greek Symbols	m	Model
α	Volume fraction of fluid	p	Prototype
μ	Dynamic viscosity		

A formal definition is as follows [7]:

a. A model and prototype are geometrically similar if and only if all body dimensions in all three coordinates have the same linear scale ratio. Then geometric similarity requires that all homologous points be related by the same linear scale ratio. This applies to the fluid geometry as well as the model geometry. All angles are preserved in geometric similarity. All flow directions are preserved. The orientations of model and prototype with respect to the surroundings must be identical.

b. Kinematic similarity requires that the model and prototype have the same length scale ratio and the same time scale ratio. The result is that the velocity scale ratio will be the same for both. As Langhaar [8] states it: The motions of two systems are kinematically similar if homologous particles lie at homologous points at homologous times. Length scale equivalence simply implies geometric similarity, but time scale equivalence may require additional dynamic considerations such as equivalence of the Reynolds and Mach numbers.

c. Dynamic similarity exists when the model and the prototype have the same length scale ratio, time scale ratio, and force scale (or mass scale) ratio. Again geometric similarity is a first requirement; without it, proceed no further. Then dynamic similarity exists, simultaneous with kinematic similarity, if the model and prototype force and pressure coefficients are identical. This is ensured if:

1. For compressible flow, the model and prototype Reynolds number and Mach number and specific-heat ratio are correspondingly equal.
2. For incompressible flow:

a. With no free surface: model and prototype Reynolds numbers are equal.

b. With a free surface: model and prototype Reynolds number, Froude number, and (if necessary) Weber number and cavitation number are correspondingly equal.

The most basic rule of dimensional analysis is that of dimensional homogeneity, and Buckingham π theorem is one of its important theories [9-10].

Two-phase flows follow the rules of fluid mechanics; however, in comparison to single-phase flows, there are many factors which contribute to the uncertainty and complexity of two-phase flows. Thus, two-phase flows are extremely complex (Even one –dimensional two-phase flows inside the tube). To overcome these complexities, researchers have taken various approaches such as experimenting on simple physical models so that they could be used in the analysis of engineering and scientific problems and finding simpler equations [11].

Generally, by categorizing different states of intersections between gas and liquid phases, which is called Regime or Flow Pattern, it will be possible to describe and interpret these types of flows. It should be noted that Flow Regimes usually are affected by tube position and its geometric shape, flow direction, physical characteristics and flow intensity of each phase, and heat flux entered into the walls of the tube [12].

Recently, many researchers experimentally and theoretically analyzed the influences of Venturi tube structural parameters on the velocity and pressure of the inner fluid. Rodio and Congedo proposed a set of optimized parameters of the venture tube by means of the cavitation's model [13]. Gupta et al. carried out an experiment of air–water two–phase fluid flowing through a venturi channel in a 700MWe Indian Pressurized Heavy Reactor and found that a two-phase flow multiplier increases as the void fraction ascends [14]. With an experimental and theoretical method, parameters of the venturi scrubber were investigated, including the throat pressure drop, the droplet dispersion and the dust collection efficiency. Among the separameters, the pressure drop is a function of the gas-liquid ratio, the throat gas velocity and the throat area [15-17]. The effects of nozzle geometry and the fluid mass flux on the fume collection efficiency of diesel fume scrubbing was studied by Dasand Biswas [18] and both the hydrodynamic and mass transfer performances of an emulsion loop-venturi reactor in cocurrent downflow and upflow configurations was evaluated by Gourich et al. [19]. By means of a numerical method, Zhu et al. proposed that an increment in the diffusion angle can achieve more mass flux, and gave out an optimal diffusion angle 30° [3]. Sun and Niu numerically analyzed the effects of the contraction ratio and the diffusion angle on mass flux and vacuum degree in the venture tube, and they suggested that the minimum pressure occurs at the intersection between the contraction and throat sections [20]. Given the pressure difference between the inlet and outlet of the venturi tube, an increase of the inlet pressure makes a throat pressure reduce. Moreover, given an inlet pressure, an increase of pressure difference between the inlet and outlet of venturi tube makes the throat pressure drop further. As both pressure difference between the inlet and outlet and the contraction ratio increases, mass flux increases as well

[3,21]. While an increase of the contraction ratio enhances the pressure loss in the venture tube [22]. They proposed that the contraction ratio ranges within 0.25–0.55 at the pressure drop of 60–83KPa. When Reynolds number is more than 2000 and the expansion ratio is more than 1.4, as the expansion ratio increases, the fluid flow appears an asymmetric distribution in the venturi tube, namely an obvious deflected flow [23]. However, few researches considered the effects of the contraction ratio and the diffusion angle on an asymmetric flow.

Manzano et al. with used of FLUENT software concluded that the relationship of diameters is the parameter that exerts the greatest influence on the head loss in the injector. Regarding the angles, it should be pointed out that the value of the nozzle does not have a significant influence, although there is a high correlation between it and the diffuser angle and they found that the rounding of junctions in the morphology between nozzle-throat and throat-diffuser junctions is the most recommended one, as it reduces head losses and delays the occurrence of cavitation [24]. J.X.Zhang has done a numerical analysis with the Fluent software in order to show pressure and velocity in the venturi tube.

He obtained that The minimum pressure occurs at the intersection between the contraction and the throat sections in the venturi tube, where pressure varies intensively. Main structural parameters that affect a pressure distribution in the venturi tube involve of the contraction ratio, the diffusion angle and the pressure difference between the inlet and outlet, as the inlet and outlet pressure difference increases, the minimum pressure increases, causing a backflow phenomenon.

He obtained that the main structural parameters affecting velocity in the Venturi tube are the contraction ratio and the inlet and outlet pressure difference. As the contraction ratio increases, the velocity in the Venturi tube ascends rapidly, and the velocity full development length in the diffusion section becomes shorter. With the increasing of the inlet and outlet pressure difference, the velocity in the venturi tube gradually increases. While the ratio of throat section length to diameter affects slightly the velocity. When the contraction ratio is less than 0.2 or the diffusion angle is less than 35°, the velocity shows an asymmetric distribution in the venturi tube [25].

Bubbles with 10 to 30 μm diameter are called Micro-Bubbles.

Numerical analysis of Micro-Bubble formation inside venturi tube requires time and large storage space and has not been yet studied numerically and all of studies is about velocity and pressure. For studying Micro-Bubbles, it is necessary to transform the mesh dimensions into micro sizes.

Changing mesh dimensions into micro size extends analysis time and necessitate large storage space for saving data. For this aim, dimensions of the model under study in this research have been minimized to the extent that micro mesh dimensions are achieved. To this end, we have used numerical similarity. Reynolds number and Euler number are the most appropriate candidates for this purpose.

Modelling Description and Numerical Solution

Flow in a Venturi tube was numerically simulated for a geometry given in Figure 1. The conduit is composed of the contraction section, the throat section, and the diffusion section. The diameter of the tube is 2.54 cm and the diameter of the throat section is 0.254 cm. A half part of the input was allocated for air inlet and the other half was allocated for water inlet. The length of throat section is 2.54 cm.

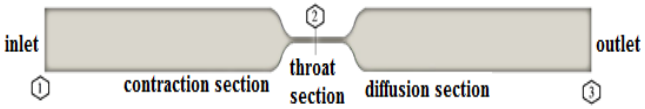

Fig. 1. Schematic of the venturi tube structure

OpenFOAM is an open-source computational fluid dynamic toolbox, written in C++ that is capable of modelling many types of problems including Partial Differential equations. OpenFOAM is also capable of solving a range of simple to complex numerical fluid flow problems. OpenFOAM has solvers which can be developed and edited further. It employs Finite-Volume Method (FVM) in solving Partial Differential equations.

Gambit software was used in constructing geometry and meshing the model. For showing the results graphically, ParaView software was used. For solving, we used InterFOAM solver which is embedded in OpenFOAM software.

This solver is used in modelling two-phase fluid flow and it is based on the shared surface control, that the ratio of the phases is determined by Volume-of-Fluid method (VOF). In the VOF method, solving the flow is done by Momentum and continuity equation [26].

The Reynolds-averaged Navier–Stokes equations (RANS) in Cartesian coordinate system are as follows [27]:

Continuity equation

$$\frac{\partial \rho}{\partial t} + \frac{\partial (\rho u_i)}{\partial x_i} = 0 \tag{1}$$

Momentum equation

$$\frac{\partial (\rho u_i)}{\partial \mathrm{t}} + \rho \frac{\partial}{\partial x_j}\left(u_i u_j\right) = -\frac{\partial P}{\partial x_i} + \frac{\partial}{\partial x_j}\left[\mu\left(\frac{\partial u_i}{\partial x_j} - \rho\overline{\acute{u}_i \acute{u}_j}\right)\right] \tag{2}$$

where,$u_i$is the average velocity towards *i*, ρ is water density, *P* is the static pressure,μ is the viscosity, $-\rho\overline{\acute{u}_i \acute{u}_j}$ is the Reynolds stress, and *i,j=1,2,3(x,y,z).*

The relationship between Reynolds stress and changes in average velocity is given by

Boussinesq hypothesis

$$-\rho\overline{\acute{u}_\iota\acute{u}_j} = \mu_t\left(\frac{\partial\overline{u}_\iota}{\partial x_j}+\frac{\partial\overline{u}_j}{\partial x_i}\right)-\frac{2}{3}\delta_{ij}\rho k \tag{3}$$

where μ_t and k are turbulent viscosity (eddy viscosity) and turbulent kinetic energy , respectively. Equations for turbulent Kinetic energy (κ) and dissipation rate of turbulent kinetic energy (ε) in standard κ-ε model are as follows:

Turbulent kinetic energy equation:

$$\frac{\partial}{\partial t}(\rho k)+\frac{\partial}{\partial X_i}(\rho k U_i)=\frac{\partial}{\partial X_j}\left[\left(\mu+\frac{\mu_t}{\sigma_k}\right)\frac{\partial k}{\partial X_i}\right] +G_k+G_b-\rho\varepsilon-Y_M \tag{4}$$

dissipation equation:

$$\frac{\partial}{\partial t}(\rho\varepsilon)+\frac{\partial}{\partial X_i}(\rho\varepsilon U_i)=\frac{\partial}{\partial X_j}\left[\left(\mu+\frac{\mu_t}{\sigma_\varepsilon}\right)\frac{\partial\varepsilon}{\partial X_i}\right]+ C_{1\varepsilon}\frac{\varepsilon}{k}(G_k+C_{3\varepsilon}G_b)+C_{2\varepsilon}\rho\frac{\varepsilon^2}{k} \tag{5}$$

where,

$$\mu_t=\rho C_\mu\frac{k^2}{\varepsilon} \tag{6}$$

In the equations above G_k and G_b are the production rate of turbulent kinetic energy due to floating and velocity changes, Y_M is dilatation dissipation, $C_{1\varepsilon}$,$C_{2\varepsilon}$,$C_{3\varepsilon}$, and C_μ are fixed values, σ_k and $\sigma_\varepsilon$are turbulent Prandtl numbers for k and ε ,respectively. OpenFOAM software uses FVM in solving equations. VOF is used for the purpose of modelling. VOF was proposed by Hirt. [28]. The method is based on the idea of a so-called fraction function α. It is a scalar function, defined as the integral of a fluid's characteristic function in the control volume, namely the volume of a computational grid cell.

The volume fraction of each fluid is tracked through every cell in the computational grid, while all fluids share a single set of momentum equations. When a cell is empty with no traced fluid inside, the value of α is zero; when the cell is full, $\alpha = 1$; and when there is a fluid interface in the cell, $0 < \alpha < 1$. The evolution of the q^{th} fluid in a system on n fluids is governed by the transport equation:

$$\frac{\partial\alpha_q}{\partial_t}+\nabla\cdot\left(U\cdot\alpha_q\right)=0 \tag{7}$$

Where, α_q is the volume fraction of fluid of q^{th} phase.

SPSS statistical software has been used to analyze the results of alpha [29-30]. Reynolds and Euler numbers should be used for dimensional analysis. Mesh dimensions in the basic models has been set to 0.1 cm. Bubbles having diameter less than 30 μm are called Micro-Bubble. In order to reach mesh dimensions in micro level and detecting Micro-Bubbles, we have to minimize the prototype until mesh dimensions are reduced to 30 μm. It means that basic model should be 0.03 times smaller.

By Reynolds number we will have

$$Re_m = Re_p$$
$$\left(\frac{\rho_{VD}}{\mu}\right)_m=\left(\frac{\rho_{VD}}{\mu}\right)_p \tag{8}$$

In this relations, *m* is model and p is prototype.

Regarding the fact that both fluid models are liquid and gas, then we have:

$$(VD)_m=(VD)_p$$
$$\frac{V_m}{V_p}=\frac{D_p}{D_m}=\frac{0.1}{0.003}=33.3 \tag{9}$$

Using Euler number we will have :

$$Eu=\left(\frac{P}{\rho_{V^2}}\right) \tag{10}$$

$$\left(\frac{P}{\rho_{V^2}}\right)_m=\left(\frac{P}{\rho_{V^2}}\right)_p \tag{11}$$

$$\frac{P_m}{P_p}=\left(\frac{V_m}{V_p}\right)^2$$
$$\frac{P_m}{P_p}=(\frac{33.3}{1})^2=1108.89 \tag{12}$$

In this paper, in order to study flow regimes in model and prototype, simulations of liquid and gas flow were made by various velocities based on Table 1.

Table 1
Velocity of air and water phase in venturi tube.

	Models Number	Vair (m/s)	Vwater (m/s)
Models (scaled models)	Model 1	3.33	16.65
	Model 2	3.33	33.3
	Model 3	3.33	66.6
	Model 4	3.33	166.5
	Model 5	3.33	333
Prototypes (basic models)	Model 6	0.1	0.5
	Model 7	0.1	1
	Model 8	0.1	2
	Model 9	0.1	5
	Model 10	0.1	10

RESULTS AND DISCUSSION

Figure 2 shows the velocity distribution and curves of velocity changes in the center of Venturi tube in scaled models (Models 1-5) and prototypes (Models 6-10). According to equation 9, the velocity in scaled models should be 33.3 times faster than prototypes. Considering the curves of velocity changes in the center of Venturi tube, changes in scaled models and real models are closely matched.

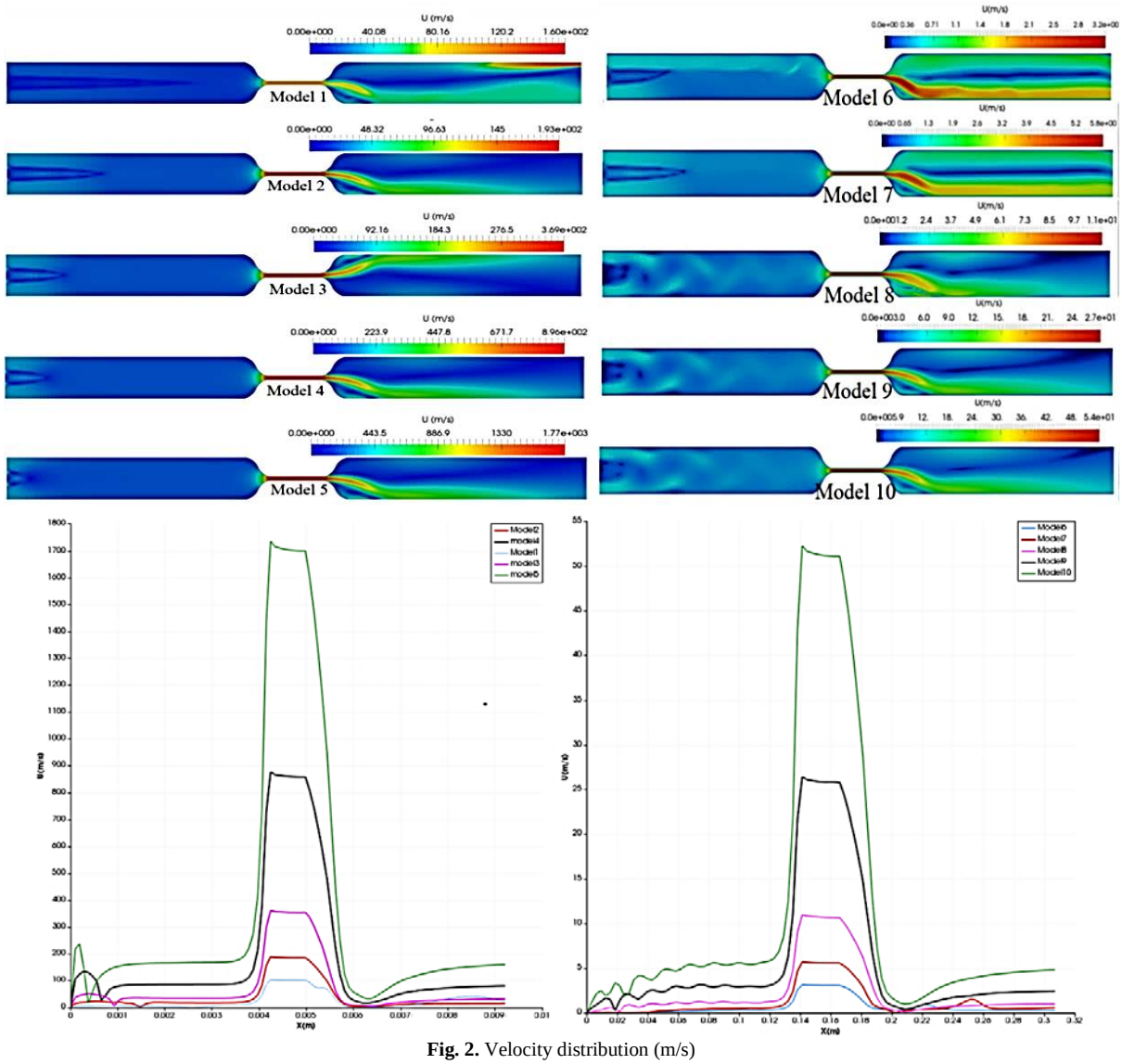

Fig. 2. Velocity distribution (m/s)

According to the results in Figure 2 and Table 2, it is seen that the maximum velocity in models 1-5 and the corresponding Models 6-10 is completely consistent with equation 9. For example, the maximum velocity in the Model 1 is 104m / s and the maximum speed in the Model 6 is 3.12 m / s, that is, the maximum velocity in the scaled model is 33.33 times the maximum velocity in the prototype.

The minimum velocity in Models 1 and 2 and Models 6 and 7 does not correspond to equation 9, but the results from the Models 3-5 and their corresponding models (Models 8-10) are completely consistent with the equation 9, for example, the minimum velocity in the Model 3 is 3.33m / s and in the Model 8 is 0.1m / s. The results show that when the water velocity is more than 2m / s, the results of the velocity analysis and flow regimes in the scaled model are thoroughly consistent with the prototype.

Figure 3 shows the pressure distribution and curves of pressure changes in the center of Venturi tube in scaled models (Models 1-5) and prototypes (Models 6-10). According to equation 12, the pressure in scaled models should be 1100 times more than prototypes.

Table 2
Pressure difference, maximum and minimum velocity.

Modes	Vair (m/s)	Vwater (m/s)	Vmax (m/s)	Vmin (m/s)	p1 (Pa)	p2 (Pa)	p3 (Pa)	Δp1=p1-p2	Δp2=p1-p3	Δp3=p3-p2
mode1	3.33	16.65	104	0.2	4.34E+06	-1.27E+06	0	5.61E+06	4.34E+06	1.27E+06
model2	3.33	33.3	189	2.9	1.38E+07	-6.12E+06	0	1.99E+07	1.38E+07	6.12E+06
model3	3.33	66.6	361	3.33	5.32E+07	-2.07E+07	0	7.39E+07	5.32E+07	2.07E+07
model4	3.33	166.5	877	3.33	2.93E+08	-1.39E+08	0	4.32E+08	2.93E+08	1.39E+08
model5	3.33	333	1735	3.33	1.18E+09	-5.47E+08	0	1.73E+09	1.18E+09	5.47E+08
model6	0.1	0.5	3.12	0.02	4646.6	-1190.97	0	5.84E+03	4.65E+03	1.19E+03
model7	0.1	1	5.7	0.048	13510.5	-4294.15	0	1.78E+04	1.35E+04	4.29E+03
model8	0.1	2	10.86	0.1	45342.7	-20589.2	0	6.59E+04	4.53E+04	2.06E+04
model9	0.1	5	26.39	0.1	270252	-123505	0	3.94E+05	2.70E+05	1.24E+05
model10	0.1	10	52	0.1	1032760	-494102	0	1.53E+06	1.03E+06	4.94E+05

The results shown in Table 2 and the graphs shown in Figure 4 also show that the pressure difference at points 1, 2 and 3, and the slope of the pressure variations in the scaled models are consistent with the prototypes.

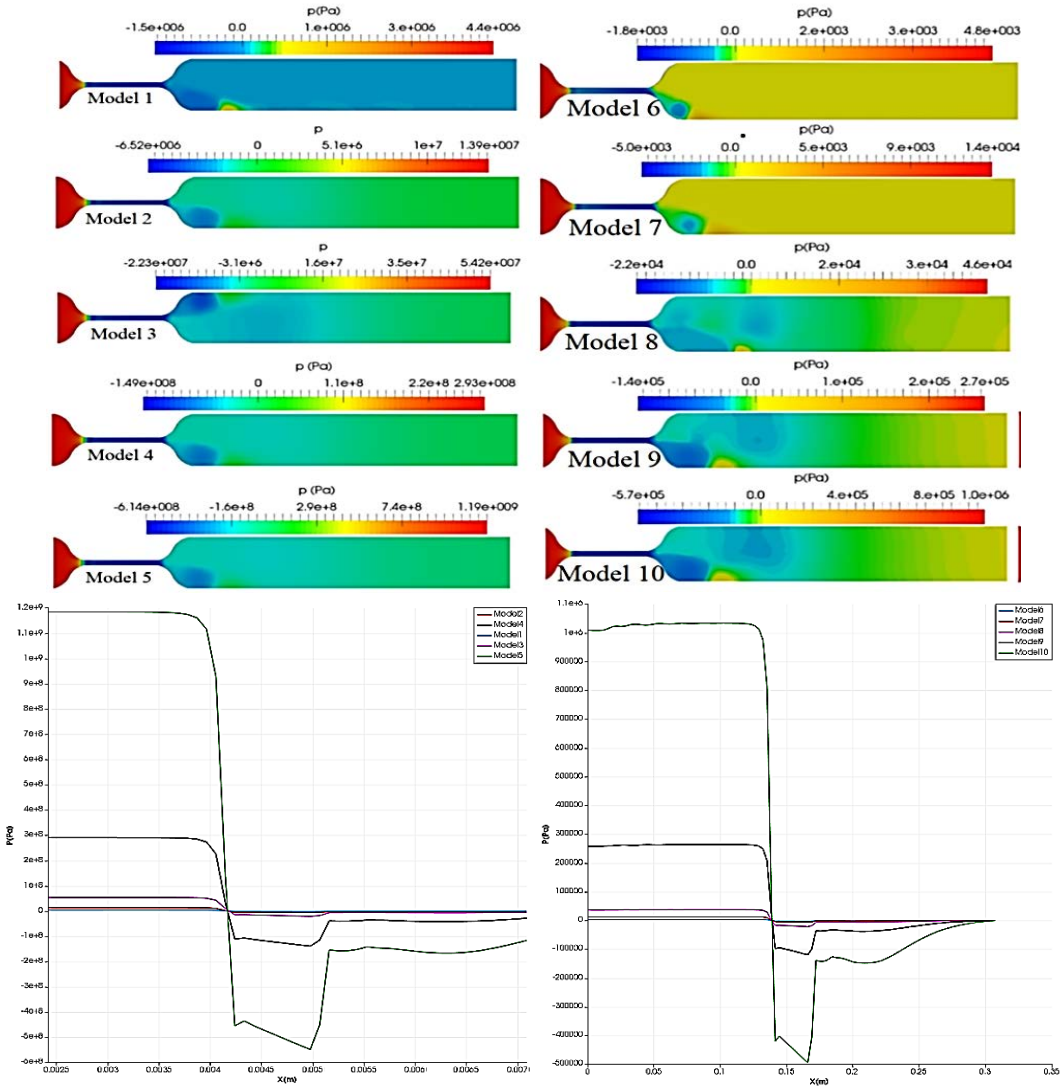

Fig. 3. Pressure distribution (Pa)

The pressure variations in the scaled models are approximately 1,100 times the pressure variations in the prototypes under study, for example, ΔP1 in model 4 is 4.32E + 8 and in the Model 9 3.94E + 5, which is 1096 times smaller. Therefore, it can be concluded that the pressure distribution is also consistent in the scaled models and the prototypes**.**

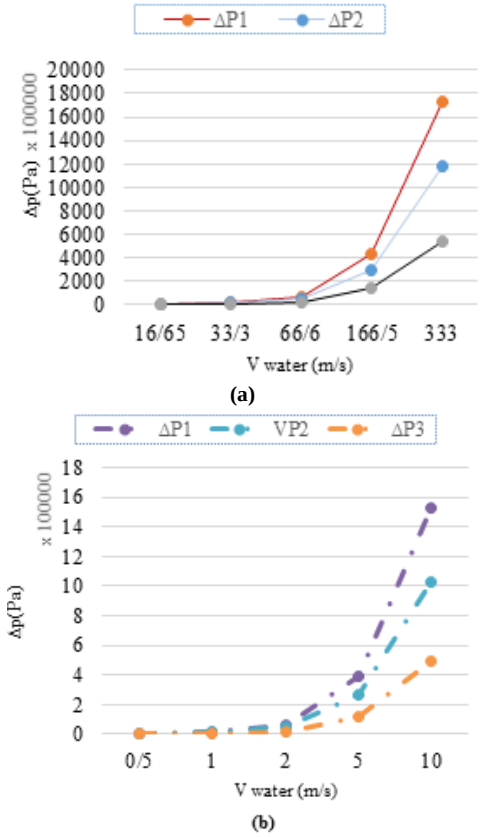

Fig. 4. Δp1=p1-p2, Δp2=p1-p3 and Δp3=p3-p2 for different values of velocity in (a) scaled models and (b) Prototypes

Figure 3 shows that the minimum pressure occurs at the intersection between the contraction and the throat sections in the venturi tube and this is completely consistent with J. X. Zhang's [25], and Sun's [20] findings. In this research, we study flow regimes inside venturi tube concerning Micro-bubble formation in the basic and scaled model, using VOF method.

Figure 2 shows the distribution of alpha along the venture tube and flow regimes for Models 1-10. Also, as shown in Figures 2 and 3, since the the contraction ratio is less than 0.2, the velocity and pressure distribution of the scaled models and prototypes studied are asymmetric, and this is completely consistent with J. X. Zhang's [25] findings**.** Figure 5 shows the results of the distribution of α and flow regimes for the scaled models and the prototypes examined. SPSS statistical software has been used to analyze the alpha.

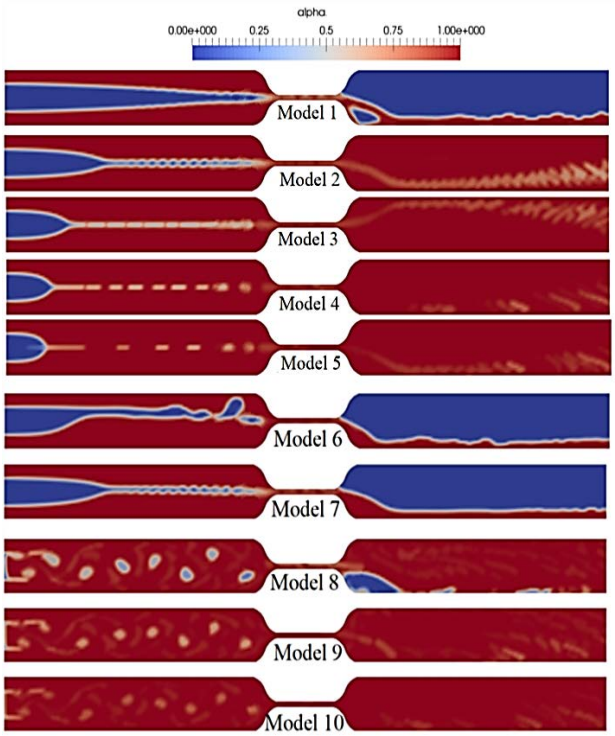

Fig. 5. Alpha distribution for models 1-10, alpha=1 means water and alpha=0 means air. Models 1-5 are scaled models and models 6-10 are prototypes

The mean and standard deviation of alpha values and results of K-S test (Kolmogorov-Smirnov Test) for the models 1-10 are presented in Table 3**.**

Table 3
results of One-Sample Kolmogorov-Smirnov Test.

		Model1	**Model2**	**Model3**	**Model4**	**Model5**	**Model6**	**Model7**	**Model8**	**Model9**	**Model10**
N		6739	6739	6739	6739	6739	6739	6739	6739	6739	6739
Normal Parameters[a,b]	Mean	.4347	.8807	.9274	.9534	.9722	.4746	.5066	.9339	.9834	.9917
	Std. Deviation	.47853	.28506	.22695	.19192	.13784	.48557	.48462	.20057	.05825	.03312
Most Extrem Differences	Absolute	.320	.395	.404	.466	.456	.303	.289	.412	.388	.401
	Positive	.320	.338	.375	.404	.420	.303	.289	.371	.388	.401
	Negative	-.244	-.395	-.404	-.466	-.456	-.274	-.286	-.412	-.339	-.368
Test Statistic		.320	.395	.404	.466	.456	.303	.289	.412	.388	.401
Asymp. Sig. (2-tailed)		.000[c]	.000[c]	.000[c]	.000[c]	.000[c]	.000[c]	.000[c]	.000[c]	.000[c]	.000[c]

a. Test distribution is Normal. b. Calculated from data. c. Lilliefors Significance Correction.

It should be noted that for all models sig <0.05, therefore, none of the models have normal distribution then so nonparametric tests should be used to analyze the results**.**

The results of statistical analysis and nonparametric correlation test are presented in Table 4.

Table 4
Results of Nonparametric Correlations.

Spearman's rho		Model1	Model2	Model3	Model4	Model5	Model6	Model7	Model8	Model9	Model10
Model1	Correlation Coefficient	1.000	.110	.328	.121	.039	.789	.875	.099	.109	.008
	Sig. (2-tailed)	.	.000	.000	.000	.001	.000	.000	.000	.000	.529
	N	6739	6739	6739	6739	6739	6739	6739	6739	6739	6739
Model2	Correlation Coefficient	.110	1.000	.404	.578	.578	.192	.183	.072	.233	.318
	Sig. (2-tailed)	.000	.	.000	.000	.000	.000	.000	.000	.000	.000
	N	6739	6739	6739	6739	6739	6739	6739	6739	6739	6739
Model3	Correlation Coefficient	.328	.404	1.000	.343	.254	.341	.385	.122	.163	.146
	Sig. (2-tailed)	.000	.000	.	.000	.000	.000	.000	.000	.000	.000
	N	6739	6739	6739	6739	6739	6739	6739	6739	6739	6739
Model4	Correlation Coefficient	.121	.578	.343	1.000	.630	.262	.217	.020	.183	.271
	Sig. (2-tailed)	.000	.000	.000	.	.000	.000	.000	.107	.000	.000
	N	6739	6739	6739	6739	6739	6739	6739	6739	6739	6739
Model5	Correlation Coefficient	.039	.578	.254	.630	1.000	.194	.098	.015	.151	.231
	Sig. (2-tailed)	.001	.000	.000	.000	.	.000	.000	.217	.000	.000
	N	6739	6739	6739	6739	6739	6739	6739	6739	6739	6739

The correlation coefficient is in the range of [-1 _1], when The closer the coefficient is to either −1 or 1, the stronger the correlation between the variables**.**

According to the results, nonparametric correlation coefficient between Models 1 and 6 is 0.789, Models 2 and 7 is 0.183 and Models 3 and 8 is equal to 0.122 and Models 4 and 8 is 0.183 and Models 5 and 10 is equal to 0.231. It is seen that only Models 1 and 6 are in good correlation. But all models have a sig <0.05, meaning the correlation of all models is meaningful**.**

CONCLUSION

This study shows, if the aim is to study the pressure and velocity in the venturi tube, the results of the scaled model

can be quite reliable. But if the goal is to study the alpha and formation of micro-Bubbles, analysis results achieved from scaled models cannot be used. Therefore, since the purpose of this study is to study micro-bubble formation in a Venturi tube and the results of alpha should also be considered, scalable models cannot be used. Then, in future studies, we need to simulate actual models in OpenFOAM software and study the formation of micro-bubbles, which will require more time and cost.

REFERENCES

[1] Zhou Y, Shun Z, Gu H, and Miao Z. Injection performance and influencing factors in self-priming Venturi scrubber. Ciesc Journal 2015;66(1):99–103.

[2] Wang X. J, Tang L, and Jiang Z. Numerical simulation of venturi ejector reactor in yellow phosphorus purification system. Nucl. Eng. 2014 Des; 268:18–23.

[3] Zhu Y, Chao MA, and Zhang XW. Study on flow in Venturi-mixer EGR for a turbo charged diesel engine.Transactions of Csice. 2002;6: 546–55.

[4] Jiang QM, Fan YN, and Yang DD. Application of venturi injector for recovering pressure energy to natural gas network. Gas & Heat. 2009;29(7): A28–A31.

[5] Quiroz-P´erez E, V´azquez-Rom´an R, Lesso-Arroyo R,Barrag´an-Hern´ VM. An approach to evaluate Venturi-device effects on gas wells production. J. Pet. Sci. Eng. 2014;116(4): 8–18.

[6] Anderson JD. Computational Fluid Dynamics: The Basics with Applications. McGraw-Hill, New York, 1995.

[7] White FM. Fluid Mechanics. Seventh Edition. McGraw-Hill, 2011.

[8] Langhaar HL. Dimensional Analysis and the Theory of Models. Wiley, New York, 1951.

[9] Shames IH. Mechanics of fluids, 4th edition, McGraw-Hill, 2003.

[10] Halliday D, Resnick R, Krane KS. Physics, Volume 1, 4th Edition, Wiley, 1992.

[11] Mattew P, Peramaki PE, Mark D, Nelson PE. The significance of two-phase flow regimes in designing multi-phase extractin systems. LBG Article, www.lbgweb.com,2000.
[12] Levy S. Two-phase flow in complex systems. John Wiley & Sons, Inc., New York, 1999.
[13] Rodio MG, Congedo PM. Robust analysis of cavitating flows in the Venturi tube. Eur.J.Mech. B/Fluids. 2014;44(2):88–99.
[14] Gupta B, Nayak AK, Kandar TK, Nair S. Investigation of air-water two phase flow through a venture. Exp. Therm. Fluid. 2016;Sci 70:148–154.
[15] Pulley RA. Modelling the performance of venturi scrubbers. Chem. Eng. J 1997;67(1):9–18.
[16] Viswanathan S. Development of a pressure drop model for a variable throat venture scrubber. Chem.Eng.J. 1998;71(2):153–160.
[17] Ahmadvand F, Talaie MR. CFD modeling of droplet dispersion in a Venturi scrubber. Chem.Eng.J. 2010;160(2):423–431.
[18] Das K, Biswas MN. Studies on ejector-venturi fume scrubber. Chem. Eng. J. 2006;119(2): 153–160.
[19] Gourich B, Vial C, Soulami MB, Zoulalian A, Ziyad M. Comparison of hydrodynamic and mass transfer performances of an emulsion loop-venturi reactor in cocurrent downflow and upflow configurations. Chem. Eng. J. 2008;140(1–3):439–447.
[20] Sun YQ, Niu WQ. Effects of Venturi structural parameters on the hydraulic performance. J. Northwest. A & F. Uni. 2010;38(2): 211–218.
[21] Qi L, Chen L. Numerical research on the hydraulic characteristics of venturi tube based on ANSYS-CFX. Tech. Super. Pet. Ind. 2014;6: 41–45.
[22] Jiang Y, Yang M, Guo C, Shen S. Numerical simulation of asymmetric flow in Venturi tube. Ciesc Journal. 2014;6(S1): 223–228.
[23] Shen SW, Yang M, Jiang YH, Wang ZY. The numerical simulation of the influence of Venturi burner's structure on rich/lean separation. Journal of Engineering Thermophysics. 2015;36(2):347–350.
[24] Manzano J, Palau CV, Azevedo BM. DE, Bomfim GV. DO, Vasconcelos DV. Geometry and Head Loss In Venturi Injectors Through Computational Fluid Dynamics. Doi:http://dx.doi.org/ 10.1590/ 1809-4430-Eng.Agric. 2016; 36(3):482-491.
[25] Zhang JX. Analysis on the effect of venturi tube structural parameters on fluid flow. AIP ADVANCES 7, 065315. 2017.
[26] Nilsson H, jasak H. source forge. OpenFOAM extension.[online], http//www.sourceforge.net.
[27] Wilcox DC. Turbulence modeling for CFD, third edition, DCW industries, Inc. 2006.
[28] Hirt CW, Nichols BD. Volume of Fluid (VOF) Method for the Dynamics of Free Boundaries. JOURNAL OF COMPUTATIONAL PHYSICS. 1981;39: 201-225.
[29] Yule GU, Kendall MG. An Introduction to the Theory of Statistics. Charles Griffin & Co.1950.14th Edition (5th Impression 1968).
[30] SCSS: A User's Guide to the SPSS Conversational Statistical System. 1980. ISBN 978-0070465336.